GNSS CONTRIBUTION TO MONITOR SEVERE RAINFALLS: AN INNOVATIVE PROCEDURE FOR WIDE AND OROGRAPHICALLY COMPLEX AREA WITH EXISTING INFRASTRUCTURES

Ilaria Ferrando

DICCA - Dipartimento di Ingegneria Civile, Chimica e Ambientale, Università degli Studi di Genova, via Montallegro 1, 16145 Genova, Italia - ilaria.ferrando@edu.unige.it

KEY WORDS: GNSS, Zenith Total Delay (ZTD), Precipitable Water Vapour (PWV), Severe Meteorological Events, GIS

ABSTRACT:

The paper presents an innovative methodology for monitoring the content of Precipitable Water Vapour (PWV) in atmosphere for wide and orographically complex area. The water vapour content is strictly related to the occurrence of rains, hence the knowledge of PWV can be useful to interpret and monitor severe meteorological events. An automatic procedure has been conceived for producing 2D PWV maps with high spatial and temporal resolution starting from Zenith Tropospheric Delay (ZTD) estimations, obtained from GNSS Permanent Stations (PSs) network compensation, and from Pressure (P) and Temperature (T) observations, all collected by existing infrastructures. In the present work both a 1D approach to analyse ZTD and PWV time series and a 2D approach to localize severe meteorological events in time and space are presented. The procedure is then applied to a wide and orographically complex area, to study two severe meteorological events occurred in Genoa with reliable results. The introduction of the Heterogeneity Index (HI), accounting the spatial variability of PWV, allows to individuate the correct timing and location of severe meteorological events.

1. INTRODUCTION

The typical application of GNSS (Global Navigation Satellite System) technology is obtaining the coordinates of a receiver by means of spatial triangulation, knowing the satellites orbits and positions. The positioning precision is affected by different sources of bias, primarily produced by the crossing of the atmosphere, due to ionospheric and tropospheric refraction, and by structural and non-structural issues (receiver/satellite clock errors, multipath, code/phase range, etc.). The Ionosphere is a dispersive layer, thus its effect depends on the frequency of the electromagnetic signal. The ionospheric bias can be easily modelled and eliminated by means of proper L1 and L2 phase combinations (iono-free model) transmitted by GNSS satellites and using the dispersion relations for Ionosphere (Spilker, 1980; Brunner and Gu, 1991). The tropospheric bias can't be reduced by means of any combination, hence it has to be taken into account. The tropospheric effect produces a bias in each satellite-receiver observation that can be related with the so-called Zenith Total Delay (ZTD), computed in the zenith direction above the GNSS station, by means of an appropriate mapping function. On the one hand, the estimation of ZTD and its time and space variability could help to enhance the positioning precision; on the other hand, the monitoring of ZTD could be useful to study and interpret severe meteorological events, as previous studies demonstrated (Bouma and Stoew, 2001; De Pondeca and Zou, 2001; Basili et al., 2003; Bock et al., 2008; Boniface et al., 2009; Bennitt and Jupp, 2012; Crespi et al., 2004; Piccardo and Sguerso, 2007; Sguerso et al., 2013, 2015; Tsuda et al., 2013).
Considering the atmosphere as a biphasic fluid composed by a mix of dry and wet gases, ZTD may be split in its two components, the Zenith Hydrostatic Delay (ZHD) and the Zenith Wet Delay (ZWD). ZHD is due to the mix of dry gases in atmosphere, is dominant (it covers about the 90% of the total tropospheric delay) and can be easily modelled by means of relations involving the atmospheric pressure and depending on latitude and elevation of the GNSS station. ZWD is due to the water vapour refractivity caused by the dipole moment of water vapour molecules and it can't be easily modelled, therefore it is typically obtained by difference between ZTD and ZHD. ZWD is closely related to the value of Precipitable Water Vapour (PWV). PWV represents the maximum amount of condensable water due to the water vapour contained in an imaginary unitary-base column that extends from the GNSS receiver height to the upper limit of the troposphere. This quantity can be considered the upper limit of the precipitable water, if the triggering conditions for water condensation are present.
PWV can be estimated above a GNSS Permanent Station (PS), by means of the relations by Bevis et al. (1992 and 1994), involving ZTD integrated with Pressure (P) and Temperature (T) observed close to the GNSS receiver.
Starting from Bevis' assumptions, a GIS procedure called G4M (GNSS for Meteorology) has been conceived to produce 2D PWV maps with high spatial and temporal resolution, using as input data GNSS, P and T sparse observations not necessarily co-located, coming from existing infrastructures.
In the present work both a 1D approach to analyse ZTD and PWV time series, and a 2D approach to produce PWV maps and to interpret their evolution are presented. The final goal is to better localize severe meteorological events in time and space for near real-time applications by means of PWV estimations.

2. GNSS METEOROLOGY

The most common instruments to measure the vertical and horizontal distribution of water vapour are radiosonde and Water Vapour Radiometers (WVR).
Radiosonde provides a good vertical resolution but it is an expensive technique, available for a restricted number of launches. Regarding the WVR, there are two main categories of instruments: the upward (UL) and the downward looking (DL). The UL WVR is a ground-based instrument measuring the microwave radiation produced by atmospheric water vapour and estimating the Integrated Water Vapour (IWV) and the Integrated Liquid Water (ILW) content along a given line of sight. The DL WVR is a space-based instrument measuring the absorption lines in the radiation from the hot background provided by the Earth. UL units can provide a good temporal coverage but they are

lacking in spatial coverage, whereas DL units have the opposite characteristics. Moreover, geostationary satellites, such as Meteosat, return images of the water vapor content, but relative to the top of the cloud layer.
GNSS signals are delayed by water vapour, dry gases, hydrometeors and other particulates in atmosphere (Neill, 1996; Solheim et al., 1999), with different effect in the Ionosphere and in the Troposphere. Thus, the GNSS technology allows to estimate the content of PWV along the zenith direction above a GNSS PS, from the ground to the upper limit of the troposphere, observing the delay of the electromagnetic GNSS signal, integrated with P and T data on the ground, as described in the following section.

2.1 Tropospheric delay estimation

The Troposphere is the closest layer to Earth, from the ground up to about 12 km, and it is the most interesting layer for GNSS signal transmission because it is the zone of active weather, where all the clouds types and meteorological precipitations develop. A mix of dry gases and water vapour constitutes it. The Troposphere's refraction is frequency independent and it is only due to temperature, pressure and relative humidity. The water vapour dipole moment contributes to atmosphere's refractivity and it is common to treat it separately from non-dipole component. The two components are commonly referred to as the wet (ZWD) and hydrostatic (ZHD); both of them assume smaller values along the zenith direction and increase with the inverse of the elevation angle's sine. The hydrostatic component is dominant and contributes for about the 90% on the total effect. On spite of the smaller effect, the wet component represents the main source of bias for its larger variability and more difficult predictability with respect to theoretical models and meteorological measurements from surface (Resch, 1984; Tralli et al., 1988).
Having surface pressure measurements, Saastamoinen (1972) showed that it is possible to model ZHD with reliable accuracy (in the order of a few millimeters), as long as the accuracy of pressure measurement is higher than 0.3 hPa.
Elgered et al. (1991) proposed the following relation

$$ZHD = \frac{(2.2779 \pm 0.0024) \cdot P_s}{f(\varphi, H)} \quad (1)$$

where ZHD is measured in mm, P_s is the surface level pressure (in hPa) and $f(\varphi, H)$ is a function accounting for the gravitational acceleration variation depending on the latitude φ and the height H on the ellipsoid (measured in km).

$$f(\varphi, H) = 1 - 0.00266 \cdot \cos(2\varphi) - 0.00028 \cdot H \quad (2)$$

Davis et al. (1985) suggested

$$ZWD = 10^{-6} \cdot \left(k_2' \cdot \int \frac{P_V}{T} \, dz + k_3 \cdot \int \frac{P_V}{T^2} \, dz \right) \quad (3)$$

where P_v is the partial pressure of water vapour (in hPa), T is the atmospheric temperature (in K) and

$$k_2' = 17 \pm 10 \quad \left[\frac{K}{hPa}\right]$$
$$k_3 = (3.776 \pm 0.03) \cdot 10^5 \quad \left[\frac{K^2}{hPa}\right] \quad (4)$$

The predictability of ZWD by means of models and surface measurements is much lower than the ZHD one. For this reason, for GNSS Meteorology applications, ZWD is typically obtained by difference between ZTD and ZHD.
ZTD can be estimated by adjustment of GNSS receivers networks, in order to correct the delay computed in a defined time span (generally, two hours or lower) with a tropospheric model adopted in standard atmosphere conditions.
Also international and national agencies deal with the estimation of tropospheric models by elaborating GNSS Permanent Stations network (PSs) and interpolating their local estimations (Bosy et al., 2012; Karabatić et al., 2011; Pacione and Vespe, 2003; Yao et al., 2015). The spatial and temporal resolutions are suitable for climate or meteorological analysis on wide area, but are too low for the monitoring of an intense localized event, as the purpose of the author.

2.2 Precipitable Water Vapour estimation

Once ZWD has been obtained, it is possible to estimate PWV, using the relation proposed by Bevis et al. (1992)

$$PWV = \Pi \cdot ZWD \quad (5)$$

where Π is a function of the physical parameters and the weighted mean temperature of the atmosphere T_m.
The proposed relation for Π is

$$\frac{1}{\Pi} = 10^{-6} \cdot \left(k_2' + \frac{k_3}{T_m} \right) \cdot R_V \cdot \rho \quad (6)$$

where R_v is the specific gas constant for water vapour and ρ is the density of water.
Davis et al. (1985) defined the weighted mean T_m as

$$T_m = \frac{\int \frac{P_V}{T} \, dz}{\int \frac{P_V}{T^2} \, dz} \quad (7)$$

representing the average temperature of atmosphere weighted by the pressure of water vapour, and depending on surface temperature, Troposphere's temperature profile and vertical distribution of water vapour. As already stated, it is difficult to estimate the partial pressure of vapour P_v and the temperature T, thus an approximate expression for the weighted mean temperature T_m has been found (Bevis et al., 1992):

$$T_m = 70.2 + 0.72 \cdot T_S \quad (8)$$

The previous (1-8) equations represent the basic equations of GNSS Meteorology and demonstrate the possibility of retrieve PWV spatio-temporal distribution in the atmosphere by means of GNSS observations.

2.3 PVW Variance Propagation

PWV variance propagation has been performed by the author to understand the role of each component and its uncertainty, and to evaluate the final rms (σ) of PWV.
Assuming ZTD rms equal to 3 mm (as suggested by Bevis et al., 1992), a latitude of 45° and a height of 1000 m known with high precision ($\sigma_\varphi = \sigma_z = 0$), a precautionary value of $\sigma_P = 1$ hPa, considering that PSs and meteorological stations are not co-located, the ZHD and ZWD variance results equal to $5.185 \cdot 10^{-3}$ mm^2 and to 14.185 mm^2 respectively.
Supposing ρ and R_v known with high precision ($\sigma_\rho = \sigma_{Rv} = 0$), assuming $T_m = 279$ K, $\sigma^2_T = 1$ K, the typical values for k'_2, k_3 and their relative σ (Bevis et al, 1992) and a conservative value of 250 mm for ZWD, it follows σ_{PWV}=0.736 mm.

2.4 PWV sensitivity analysis

To evaluate how much PWV is sensitive to the variation of the parameters involved, a sensitivity analysis has been carried out using a MATLAB code. The code is intended to produce two graphs representing the variation of PWV and σ_{PWV} varying one of the parameters. The tolerance interval is discretized in seven

points, to compute the corresponding PWV in: the default value and in the default value $\pm 3\cdot\sigma$, $\pm 2\cdot\sigma$ and $\pm \sigma$.
Table 1 reports PWV and σ_{PWV} sensitivity to the variation of the different parameters inside their tolerance intervals, assuming φ = 45°, z = 1000 m, the default values for the variables (k'_2 = 17 K/mbar, $k_3 = 3.776\cdot10^5$ K^2/mbar, T_m = 281.27 K, P = 1013.25 hPa, ZTD = 2.5 m) and the corresponding σ (as reported in equation (4) and section 2.3).
PWV and σ_{PWV} variations are quite limited if the five variables variations are limited inside the corresponding tolerance intervals. P and ZTD are the most influencing parameters on PWV values. In fact, a variation of about 6 hPa in P produces a variation of PWV of about 2 mm; a variation of 9 mm in ZTD produces a variation of 3 mm in PWV.

Variab.	Conf. interval	PWV [mm]		σ_{PWV} [mm]	
		Min	Max	Min	Max
k'_2	(7;27)	31.0	31.5	$6.9\cdot10^{-1}$	$7.0\cdot10^{-1}$
k_3	$(3.68;3.87)\cdot10^5$	30.5	32.0	$6.7\cdot10^{-1}$	$7.1\cdot10^{-1}$
T_m	(279.1;283.4)	31.0	31.5	$6.9\cdot10^{-1}$	$7.0\cdot10^{-1}$
P	(1010;1016)	30.0	32.2	$6.9\cdot10^{-1}$	$7.0\cdot10^{-1}$
ZTD	(2.491;2.500)	29.7	32.7	$6.8\cdot10^{-1}$	$7.0\cdot10^{-1}$

Table 1. PWV and σ_{PWV} sensitivity as each parameter changes around the default value

3. DATA NETWORKS AND DATABASE

The GNSS Meteorology applications that have 2D PWV maps as final product mainly exploit existing national networks or specifically designed high dense (1-2 km) GNSS networks (Sato et al., 2013).
An element of innovation in this field has been introduced by Andrea Walpersdorf, who proposed to use existing regional, national and international GNSS PSs for the retrieval of ZTD, to be used in climatological applications (Sguerso et al., 2013).
The present research proposes to estimate PWV using these GNSS networks, together with NOAA existing network of P and T observations. Note that GNSS receivers and P and T sensors are not necessarily co-located. To overcome the low density and the sparseness of the networks, their different configurations and distribution, a simplified mathematical model was conceived (Sguerso et al., 2014). A detailed description of networks and data follows.

3.1 GNSS Permanent Stations Network

GNSS data of 181 PSs, belonging to global (IGS and EUREF), trans-national (GAIN), national (France: RENAG and RGP; Switzerland: AGNES; Italy: GEODAF and RING) and regional (Piemonte and Liguria) networks, covering the French-Italian neighbouring area, have been used to estimate a set of homogeneous tropospheric parameters (ZTDs, horizontal North-South and East-West tropospheric gradients) through common elaboration techniques and procedures. The average data spacing is 40 km. The total extent is depicted in Figure 1.

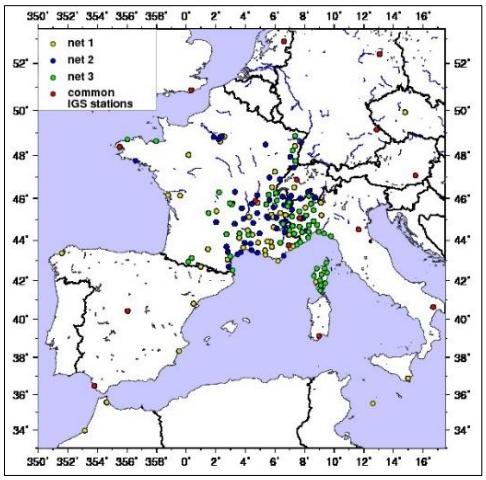

Figure 1. Total extent of GNSS PSs network

The GAMIT/GLOBK software ver. 10.4 and 10.6 (Herring et al., 2010, 2015) was employed to elaborate the GNSS data. Due to computational limits of GAMIT/GLOBK software, the PSs network has been split in three sub-networks according to decreasing station age (net1, net2 and net3, respectively), to obtain stable network geometries. A common set of 15 stations was included in each sub-network in order to achieve a stable reference frame. Within these 15 stations, 13 belong to IGS and 2 to EUREF networks.
To estimate the total amount of ZTD, several IGS stations at large distances (more than 1500 km, according to Tregoning et al., 1998) from the local network were included in each analysis.

3.2 ZTD estimations and validation

The ZTDs and the gradients were estimated for each station, simultaneously with a daily positioning solution for 24 hours sessions and were extracted from the ambiguity free solution, in order not to introduce biases in ZTDs (Santerre, 1991; Walpersdorf et al., 2007). The settings implemented for the ZTD estimations are described in Sguerso et al. (2013, 2015).
The ZTD estimations have been validated by means of two strategies: an intra-net comparison of ZTDs from the 13 IGS and the 2 EUREF common PSs, and a comparison with IGS's official ZTD estimations. Both of them result extremely useful to check the coherence of tropospheric parameters evaluated in different networks and to understand how much the network, in which a PS is included, can influence the determination of the tropospheric parameters.
3.2.1 Intra-net comparison: The 15 common PSs have been used to verify the internal consistency between the three networks calculations.
Table 2 reports the average differences and standard deviation values for the entire year 2011, for the 15 PSs. Table 3 reports the average and maximum number and percentage of outliers.

Intra-net comparison (2011)		
	With outliers	Without outliers
Average difference [mm]	net1-net2 = 0.4	net1-net2 = 0.4
	net1-net3 = 1.4	net1-net3 = 1.4
	net2-net3 = 0.9	net2-net3 = 0.9
Standard deviation [mm]	net1-net2 = 1.8	net1-net2 = 1.6
	net1-net3 = 2.0	net1-net3 = 1.7
	net2-net3 = 1.9	net2-net3 = 1.6
Max and min differences [mm]	net1-net2 = (-48;26)	net1-net2 = (-6;8)
	net1-net3 = (-67;56)	net1-net3 = (-5;8)
	net2-net3 = (-70;55)	net2-net3 = (-6;7)

Table 2. Comparison of ZTDs for the common 15 PSs for 2011

Intra-net comparison (2011)	
Without outliers	
Average number of outliers	net1-net2 = 58 (1.4%)
	net1-net3 = 69 (1.6%)
	net2-net3 = 66 (1.6%)
Maximum number of outliers	net1-net2 = 82 (1.9% SFER)
	net1-net3 = 182 (4.5% TORI)
	net2-net3 = 175 (4.3% TORI)

Table 3. Average and maximum number of outliers

The average difference values are quite small and almost the same considering or excluding the outliers. The standard deviations slightly decrease removing the outliers. Instead, the maximum and minimum values of the differences reduce substantially if the outliers are removed. This means that the ZTD estimates are coherent between the three sub-networks, with differences within the typical errors of 3-5 mm.
The average number of outliers is almost the same in the three comparisons, with slightly better results for net1-net2; the same behaviour is confirmed in the maximum number of outliers.

3.2.2 Comparison with IGS's official ZTD estimates: The comparison with IGS's official troposphere product was performed for year 2002 on 16 PSs; the ZTD estimates were extracted from net1 elaboration.
Globally, the comparison shows total differences with a mean bias of -3.6 mm and a standard deviation of 4.5 mm. The persistent bias could be related to the different network configurations, to the lack of constrain in any a priori position in the regional network elaboration, and to possible differences in the troposphere models used in the two solutions. Additionally, the different time spans at which the two ZTD estimations are carried out (5 minutes for IGS solutions and 2 hours for GAMIT solutions) could influence the results. Nevertheless, the observed constant bias does not diminish the capacity of investigating the evolution of ZTD in time.

3.3 ZTD DataBase

The two-hourly ZTD estimations and three-hourly tropospheric gradients for the 181 PSs have been included in the RENAG DataBase (DB). A first release containing ZTD and gradients from January 1998 to May 2012 was already available (Sguerso et al., 2013). A recent update was performed until December 2015. The complete DB, that will contain two-hourly ZTD estimates and couples of N-S and E-W gradients over 18 years, will be available soon. The DB will allow ZTD/gradient trend estimation and conversion from ZTD to PWV, if integrated with P and T observations.

3.4 Pressure and Temperature data

Following the criterion of exploiting existing infrastructures, a selected number of NOAA P and T stations in the French-Italian border region has been chosen. P and T sensors are not always co-located. Moreover, occasional lack of P or T data may happen due to maintenance or malfunction of the stations. For these reasons, the density of the networks varies in time.

4. ZTD AND PWV 1D ANALYSIS

As mentioned in section 2, starting from the two-hourly ZTD estimates, it is possible to calculate two-hourly PWV introducing P and T observations in the same site or nearby the PSs. The availability of ZTD long time series integrated with P and T historical data, allows to obtain PWV, which is useful for the interpretation of severe meteorological events.

In the following, an application for the city of Genoa (Italy) is shown. Genoa has been chosen because historically and recently hit by intense meteorological events (e.g. 4th November 2011 and 9th October 2014).
Two PSs are present in Genoa: GENO and GENU. GENO is an IGS PS and it is located on the Navy Hydrographic Institute building, whereas GENU is one of the six PSs belonging to the Regione Liguria positioning service, and it is located on a building of DICCA Department of the University of Genoa.
GENO and GENU PSs are not equipped with P and T sensors, thus P and T data have been extracted from two Meteorological Stations (MSs) of the University of Genoa, near the PSs: the Meteorology Observatory and the Villa Cambiaso stations (hereafter DISTAV and DICCA MS respectively). Figure 2 shows the positions of the two meteorological stations, with respect to GENO and GENU PSs, which are a few km apart.

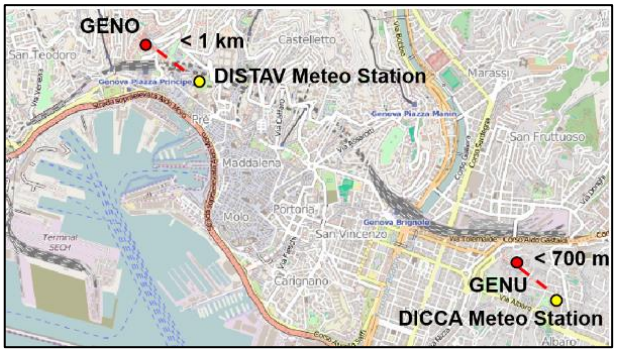

Figure 2. Genoa PSs and MSs

DISTAV MS provides hourly mean, maximum and minimum temperature and barometric pressure data from January 2002 to December 2015 at MS height (58.3 m above mean sea level). DICCA MS registers temperature, humidity, pressure, solar radiation, wind velocity and rain data since 1989 with half-hour time step, referred to MS height (40 m above mean sea level).

4.1 ZTD Time Series

In order to identify ZTD patterns related to intense precipitation events, data from 1998 for GENO and from 2009 for GENU have been analysed. The annual two-hourly ZTD time series allow to compute a climatological average of ZTD, by averaging the corresponding two-hourly estimations at the same time and the same day of different years. The climatological average can be compared with the ZTD evolution of individual years, in order to identify specific behaviours related to intense rainfalls.
In the present thesis, the climatological averages for GENO and GENU have been compared to the ZTD evolution over the year 2011. In Figure 3, the blue dots represent the climatological averages and the red dots the year 2011. The climatological averages present slightly different behaviors, probably due to the different time spans over which were computed. The 2011 ZTD time series result almost identical for the two PSs. This demonstrates that the two PSs inspect the same portion of Troposphere.
Focusing on 4th November 2011 rain event and on GENO, Figure 4 represents the climatological average of ZTD time series with error bars (black lines) related to the root mean square differences of the individual years with respect to the climatological average, superposed on the 2011 time series. Several episodes of 2011 ZTD are significantly higher than the climatological average. Among them, the Genoa storm of 4th November 2011, which is highlighted by the black vertical bars.

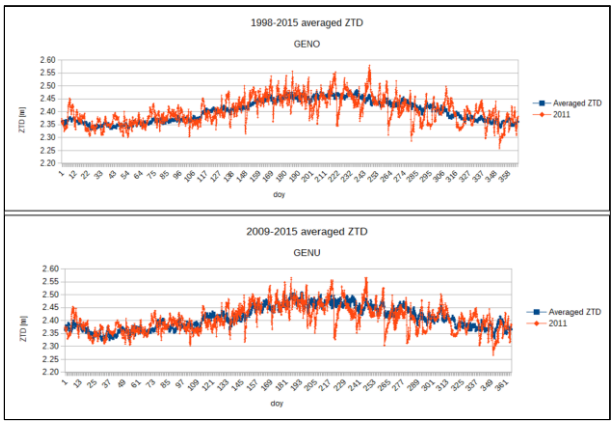

Figure 3. GENO and GENU ZTD climatological average (blue) and 2011 time series (red)

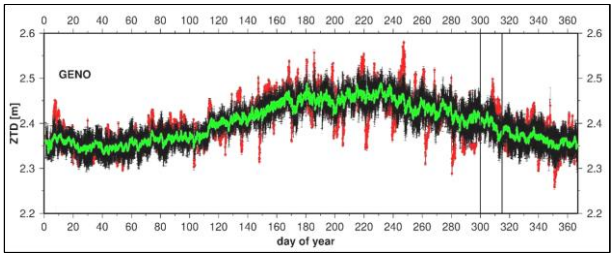

Figure 4. ZTD 2011 (red) and climatological average (green) with error bars (black) on GENO

A zoom on 4th November is depicted in Figure 5. The vertical bars underline the 4-hour interval with most of the rainfall. ZTD was significantly higher than the climatological average for about 30 hours, starting about 12 hours before the maximum of rainfall on 4th November (doy 308).

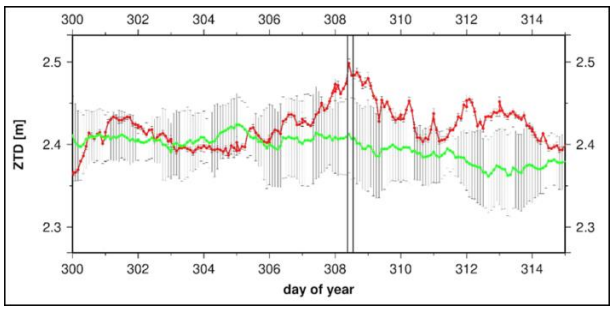

Figure 5. Zoom of ZTD time series during 4th November 2011 Genoa storm

4.2 PWV Time Series

The same approach of time series analysis was extended to PWV, to obtain a closer link to potential rain. The PWV time series from 2002 to 2015 for GENO and from 2009 to 2015 for GENU were produced, and the PWV climatological averages were computed. Focusing on 4th November 2011 rain event, Figure 6 represents the average PWV time series (in blue) and the 2011 PWV time series (in red), together with the error bars (light grey lines), showing the root mean square differences of the individual years with respect to the climatological average. There are several episodes which overcome the value of climatological average. Among them, the Genoa storm of 4th November 2011.

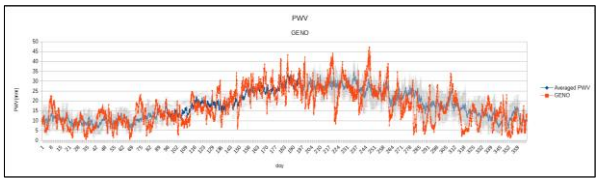

Figure 6. Climatological average (blue), 2011 PWV (red) and error bars

A zoom on shorter time span, from doy 225 (13rd August) to doy 333 (29th November), is represented in Figure 7. The two events in the circles, referring to 4th September 2011 (green circle) and to 4th November 2011 (red circle), are taken as example of the overcoming of the threshold represented by the climatological average error bars.

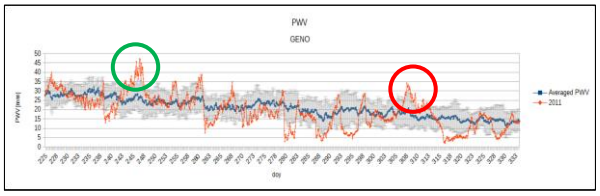

Figure 7. Zoom of PWV time series

The total amounts of rain were substantially different in the two cases. In fact, on 4th September the amount of rain was very limited and not likely to produce a meteorological alert, whereas on 4th November the amount of rain was considerably higher.
Omitting considerations on the triggering conditions, which are more related to an atmospheric physics study, the presented approach, based on the overcoming of a threshold, seems not exhaustive for individuating the occurrence of severe meteorological events. The 1D approach is still valid to characterize the pattern of PWV and it can represent a new source of available data, to deepen the knowledge of meteorological phenomena and their evolution in time and space. Even so, this strategy could be applied to other test cases in order to improve the method and identify other eventual indicators. However, a 2D methodology has been conceived to monitor the evolution of PWV in time and space.

5. PWV 2D PROCEDURE

A GIS procedure has been conceived to realize 2D maps to monitor the evolution of PWV content in atmosphere.
Using the commands of GRASS GIS ver. 6.4 and map algebra, the GNSS Meteorology equations (1-8) were simply implemented. In order to transform local ZTD, P and T information to 2D PWV maps, a simplified mathematical model, conceived to describe the atmosphere's physics, including data interpolation, was performed. Hence, the interpolated P, T and PWV maps were compared with the fields coming from the meteorological simulation, to check the adequacy of the proposed procedure. Then, an indicator for severe rainfalls was identified.

5.1 Data interpolation

A major issue was to identify the most appropriate interpolation technique to create PWV maps from ZTD, P and T data, in a quick and automatic way for near-real time application, in order to support the monitoring of intense meteorological events. The main difficulties were due to the sparse distribution of P, T and ZTD data and the different networks configurations, combined with high resolution and wide orographically complex computational region.
The meteorological event of Genoa on 4th November 2011 was a first case study to compare the interpolation techniques.

117 PSs on the French-Italian neighbouring area extracted from RENAG DB and 27 NOAA meteorological stations were employed to compare Inverse Distance Weighted (IDW), Regularized Spline with Tension (RST), kriging (krig) and Triangulated Irregular Network (TIN) interpolation techniques with low resolution.
Figure 8 depicts the distribution of the GNSS PSs, P and T networks as black, red and blue dots respectively. The mean spacing between GNSS PSs is about 40 km, while P and T stations are sparser, with a mean spacing of about 150 km.

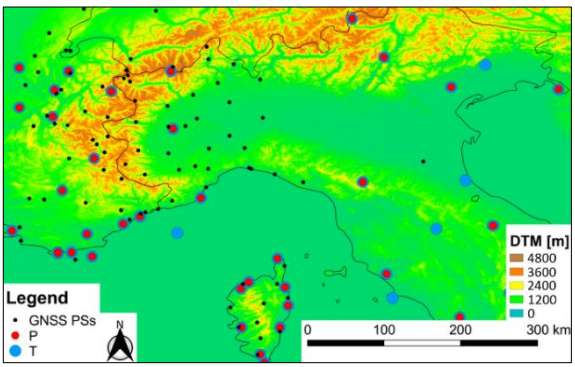

Figure 8. Distribution of GNSS, P and T stations

5.1.1 ZTD interpolation: The comparison of interpolation techniques was performed on a wide computational area with a resolution of 6' (about 10 km) on ΔZTD data, representing the differentiation in time of ZTD with respect to a "calm" moment (Ferrando et al., 2017).
The geostatistical behavior of the observed data was analysed, computing the variogram of ΔZTD in R environment (2008), to verify the correctness of the grid size of the interpolation maps. Figure 9 depicts the empirical points and the variogram model of ZTD data relative to 03/11/2011 04 UTC with respect to 03/11/2011 02 UTC.

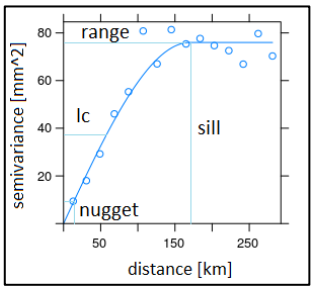

Figure 9. Variogram of ΔZTD

The variogram model that best fit the empirical data is a spherical function. The correlation length (indicated in Figure 9 as l_c) can be estimated to about 50-60 km, while the mean distance between PSs is around 40-60 km. So similar magnitudes indicate an appropriate density for the considered "regional" GNSS network, but represent the upper limit of the sampling.
ΔZTD data have been interpolated via IDW, RST, krig and TIN. In particular, for the IDW technique, three different tests have been performed using 3, 6 and 12 nearest points, indicated as IDW3, IDW6 and IDW12 respectively. Concerning RST, the smoothing parameter has been set close to zero to make the interpolated surface passing on the sampled points. The Regression Kriging (RK) was employed, also to evaluate the data correlation with elevation.
In order to define which interpolation technique could be the most representative of the ZTD spatial distribution, 12 PSs of the 117, called Check Points (CPs), were excluded by the interpolation dataset and were used to verify the results. The comparisons were carried out on the CPs, along a transept representative of the complex orography of the area to focus the attention on the altimetric differences, and through a 2D difference map between interpolated surfaces to analyze the global behavior in the study area.
Table 4 reports the minimum, maximum, mean and standard deviation of each techniques calculated on the 12 CPs.

	Min	Max	Mean	Std
IDW3	-14.9	3.1	-0.6	5.2
IDW6	-14.0	3.2	-0.7	5.0
IDW12	-14.1	4.4	-0.6	5.2
RST	-10.9	4.0	-0.6	4.1
krig	-11.3	4.0	-0.7	4.0
TIN	-11.5	3.4	-0.9	4.4

Table 4. Evaluation of different interpolation methods compared with observed values at 12 test PSs (in mm)

The values are very similar for every interpolation method, with differences between interpolated surface values and the observed values of the "check points" are always within the mean ± 3σ. Kriging and RST seem to behave slightly better, having lower values of standard deviation.
Figure 10 depicts the trace of the transept and the values of ΔZTD along it, produced applying the previous interpolation techniques. The results are quite similar, apart from IDW3 which has a trend in steps. Excluding IDW3, the maximum differences between interpolated and true values of ΔZTD are generally less than 4 mm, which is comparable to the standard deviation noise.

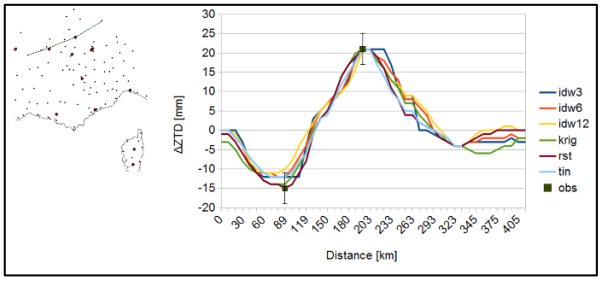

Figure 10. Transept position (on the left) and values of ΔZTD along it (on the right), from South/West to North/East

Figure 11 depicts the 2D interpolation surface of ΔZTD between using IDW6, and the differences of the various interpolation techniques in respect to IDW6.

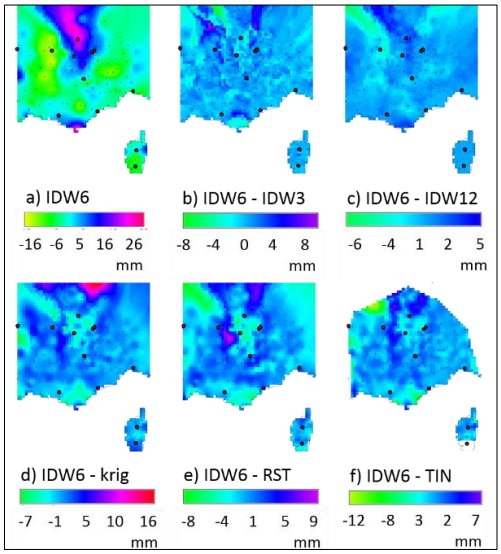

Figure 11. Map of ΔZTD created by IDW6 interpolation and difference maps between IDW6 and the other techniques

The interpolated maps seem quite similar, with main differences located at the boundary. Excluding the boundary area, the maximum differences range between -7 (IDW6-TIN) and 9 (IDW6-RST) mm. Systematic patterns are present only for IDW6-IDW3.
However, RST and kriging have been considered not suitable for near real-time applications, due to the needed calibration of their parameters (tension and smoothing for RST and the variogram for kriging), which are very sensitive to the network's configuration that can vary in time due to temporary lack of data. IDW6 parameters are less sensitive, assuming almost standard values. TIN has no parameter to be defined and shows high adaptability to different network configurations. Hence IDW6 and TIN can be successfully used for near real-time applications.

5.1.2 P and T data interpolation: P and T 2D maps were generated applying an interpolator involving a simplified mathematical model conceived by the research group (under evaluation for a patent).
Generally, P and T 2D maps could be obtained from meteorological models, but the present procedure is intended to be totally independent from weather models. Hence, interpolation of data coming from NOAA's DB of P and T meteorological stations has been carried out. In this way, the procedure results could be used as starting conditions for existing meteorological models or as comparison with them, to better understand the meteorological phenomena.
P and T data have been interpolated via IDW, RST, TIN and RK. Then, the same approach used for ZTD has been extended to P and T fields: comparisons were carried out both along a transept and 2D differences maps, to evaluate both the local and the global behaviour in the study area.
Despite the difficulties due to the sparse distribution of P and T data and the considerable orographic effect, the simplified mathematical model seems effective in reproducing P and T fields. All the tested interpolators show similar results, with higher differences located in high altitude areas, both for P and T and in the edge regions, due to the different behaviours of the tested interpolators.
For further details on the comparison results, refer to Ferrando et al. (2016).

5.2 Comparison with meteorological simulation

The interpolated P, T and PWV maps were compared with the fields coming from a meteorological simulation generated by using the entire set of existing observations.
The simulation maps were produced using the mesoscale Weather Research and Forecasting (WRF) model. The simulation settings are summarized in Cassola et al. (2015).
Again, as already done in the comparison between ZTD, P and T fields interpolated with different methods, the comparisons were carried out along a transept and through 2D difference maps.
For P and T fields, the comparison along the transept has been carried out between interpolated fields, meteorological simulation and observed data, which showed a good accordance, confirming that it is possible to obtain P and T fields even from sparse data. The comparison through 2D difference maps provides similar results in the entire study area. A deeper analysis on the results is presented in Ferrando et al. (2016).
The attention is here focused on the comparisons on PWV maps, whose validation is a recent progress but, for the sake of completeness, is here reported..
The WRF and G4M PWV data have been produced with a spatial resolution of 3.3 km and temporal resolution of 1 hour. As a consequence of what emerged from the comparison between interpolators, TIN was used to produce PWV maps.

Figures 12a and 12b depict the G4M and WRF PWV maps produced for 4th November 2011, 10 UTC; Figure 12c shows the PWV difference map. The contour lines on Figures 12a and 12b correspond to PWV values of 20, 25, 30, and 35 mm.

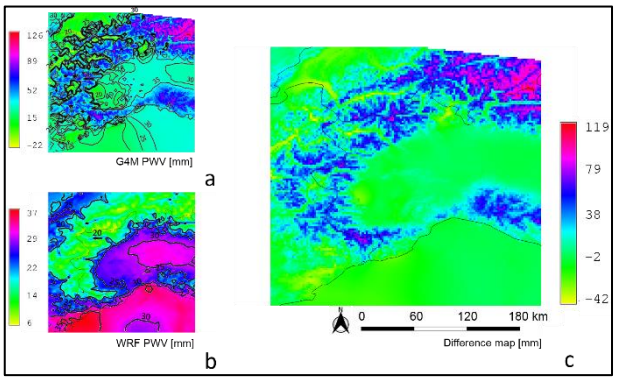

Figure 12. PWV map from the G4M procedure (a), WRF simulation (b) and difference map (G4M-WRF) (c)

The unrealistic negative PWV values in Figure 12a may be due to the effect of P overestimation and/or ZTD underestimation in localized areas. The PWV negative values have been sorted in 5 classes (from 0 to -22 mm with steps of 5 mm) and then compared with the Digital Terrain Model (DTM), to assess the influence of elevation on the unrealistic values of PWV. What firstly emerged is the non-significance of negative PWV values from a statistical point of view; in facts, they are limited to 1.6% of the total cells. They are typically located in elevation ranges from 0 to 1000 m in areas where an abrupt variation of elevation is present (e.g., valleys).

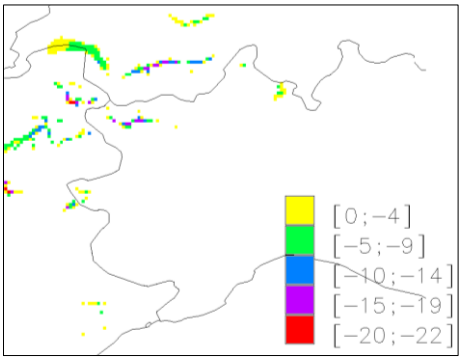

Figure 13. Distribution of PWV negative values

Two-hourly PWV time series for 3rd and 4th The PWV difference map shows large differences in high-altitude areas, whereas the differences are negligible for flat land and on the sea. The average and root-mean-square (rms) of the PWV differences are 8 mm and 24 mm, respectively. The PWV differences might be due to observation and/or interpolation errors of P and T fields, generated by the simplified mathematical model, and of the ZTD maps, in addition to WRF uncertainties.
To asses if the encountered discrepancies are significant and to determine their effect on the interpretation of the meteorological phenomenon, two strategies have been introduced: (1) the analysis of the PWV time series for PSs at different elevations, and (2) the study of PWV along a section crossing complex topographic areas.
GENO (110 m a.s.l.), TORI (261 m a.s.l.), GRAS (1270 m a.s.l.), and AGNE (2300 m a.s.l.) two-hourly PWV time series of G4M and WRF PWV have been analysed from 3rd November 2011 00 UTC to 4th November 2011 22 UTC. The two series show slight differences (few millimeters), as reported in Figure 14. This highlights the correct interpretation of the PWV temporal

evolution by G4M, in spite of the influence of orography on PWV.

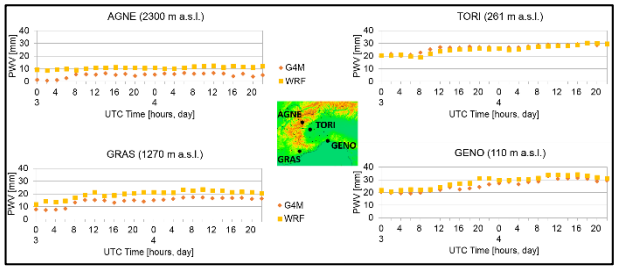

Figure 14. Two-hourly PWV time series for 3rd and 4th November 2011, for GENO, TORI, GRAS and AGNE

Then, a section of the G4M and WRF PWV maps passing through the Alps was studied. The position of the section and obtained PWV values are depicted in Figure 15. A strong orographic effect is evident in the G4M PWV map.

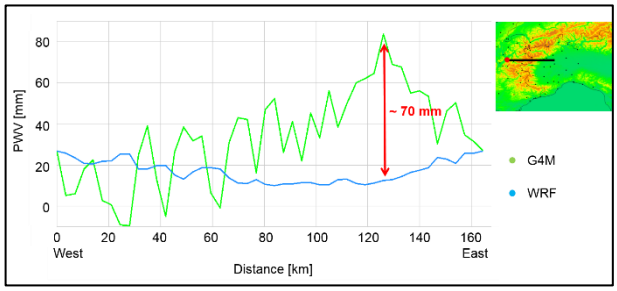

Figure 15. G4M and WRF PWV values along a transept

5.3 ΔPWV maps

To remove the orographic effect, the ΔPWV map was introduced. The ΔPWV consists of time differentiation of PWV maps with respect to a "calm" moment, when the PWV content in the atmosphere is limited. This allows to remove the orographic effect, which is constant in time, and to highlight PWV variations. Figure 16 reports the ΔPWV trend relative to the same section of Figure 15. The removal of the orographic effect and a reduction of the differences between the curves, from more than 20 mm (on average) to approximately 2–3 mm, are evident.

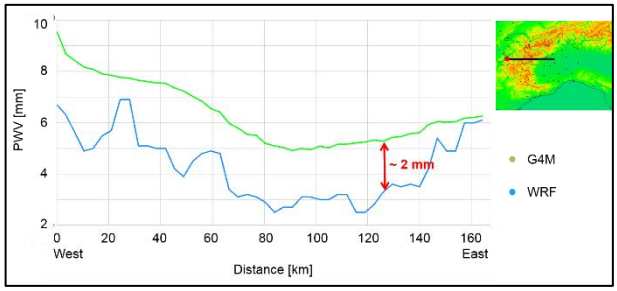

Figure 16. G4M and WRF ΔPWV values along a transept

The same effect can be globally observed in the entire study area by creating a difference map of the G4M and WRF ΔPWV maps, as shown in Figure 17c. The ΔPWV maps from G4M and WRF are depicted in Figures 17a and 17b. In spite of the differentiation in time, several differences between the two ΔPWV maps are visible, but a substantial reduction with respect to the values reported in Figure 12 can be observed. The ΔPWV differences range from -17 to 6 mm, with a mean value of -1 mm and standard deviation of 2.8 mm.

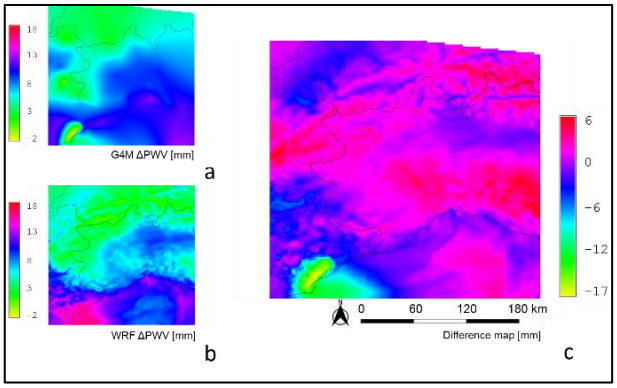

Figure 17. ΔPWV map from the G4M procedure (a), WRF simulation (b) and difference map (G4M-WRF) (c)

5.4 An indicator for severe rainfalls: Heterogeneity Index

In order to detect remarkable features in the PWV evolution, which can potentially precede severe meteorological events, and to better correlate the PWV content to the occurrence of rain, the spatial variability of PWV has been considered as a promising indicator. Indeed, the overcoming of a threshold of PWV seems a not sufficient parameter, as shown in the 1D analysis.
Moreover, the ΔPWV map does not help in defining where a severe event could take place. An example is reported in Figure 18a (relative to 4th November 2011, 10 UTC), where a severe event occurred in circle 1 and no rain occurred in circle 2, although both locations are characterized by a high ΔPWV.
The hourly cumulated rain observed on 4th November 2011, at rain gauges in circles 1 and 2 is reported in Figure 19b and 19a, respectively.

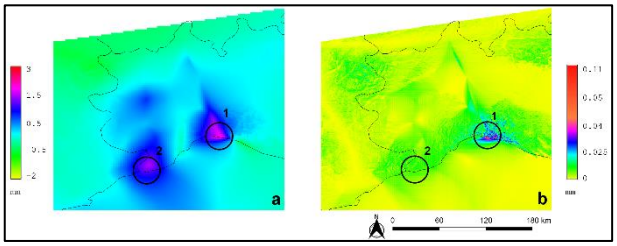

Figure 18. ΔPWV is not sufficient to determine if a severe event may occur in circles 1 or 2 (a), whereas HI highlights circle 1, where the severe event occurred (b)

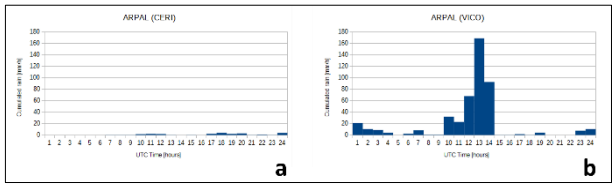

Figure 19. Hourly cumulated rain observed on 4th November 2011, at rain gauges in circles 1 (right) and 2 (left)

To localize intense meteorological events in time and space, an index accounting for the spatial ΔPWV variability, the HI, has been conceived. The index represents ΔPWV "block standard deviation" obtained by resampling of ΔPWV maps to a coarser grid (1 km) and computing the value of the standard deviation, using the GRASS module *r.resamp.stats*. Thus, each pixel of the HI map represents the empirical standard deviation of the 16 ΔPWV map pixels included in it. The 1 km resolution was deemed to be an appropriate resolution for the present case study, because it is comparable to the spatial scales of the analyzed meteorological phenomenon. Figure 18b shows high HI values

only in circle 1, where the event occurred, and not in circle 2, where no rain occurred.
As will be shown in the next section, HI seems a promising indicator to localize in time and space the occurrence of heavy rains. Thus, HI could be useful to an early-warning system based on near real-time PWV maps, as an independent contribute to meteorological alerts.
In the near future, the correlation between rainfall and HI peaks will be studied in depth, paying particular attention to the localized spatial and temporal distribution of heavy rainfall.

6. APPLICATION ON A REAL TEST CASE

During the morning of 4th November 2011, a stationary and self-healing storm developed over the city of Genoa, causing a huge amount of rain with intensities of up to 169 mm/hour near the city center. In some areas of Genoa, almost 400 mm rain fell over the entire day and ~300 mm rain fell from 09 to 13 UTC. This severe meteorological event led to the flooding of the Bisagno River and its tributary Fereggiano, causing the death of six people and much damage.
Figure 20 shows the reflectivity map observed by the Bric della Croce (Turin) meteorological radar at 11:35 UTC, where the localized distribution of intense rainfall around Genoa (circle 1) and moderate values elsewhere (e.g., circles 2 and 3) are evident.

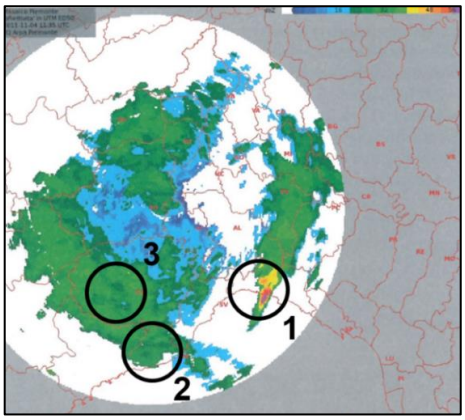

Figure 20. Reflectivity map observed by the Bric della Croce meteorological radar at 11:35 UTC on 4th November 2011

The application of the G4M procedure to this severe meteorological event based on a posteriori and simulated near real-time approaches is presented in the following Sections 6.1 and 6.2.
G4M procedure was also applied to the severe meteorological event occurred on Genoa on 9th October 2014 with satisfactory results.

6.1 PWV a posteriori monitoring

PWV maps were realized, with a time step of 2 hours to analyze the meteorological phenomenon and its evolution in space and time, from 02 UTC on 3rd November 2011 to 00 UTC on 5th November 2011, using the G4M procedure. The existing infrastructure used in the elaboration consisted of 117 PSs with a mean spacing of 40 km and 35 meteorological stations with a mean spacing of approximately 150 km. The computational region has been discretized with a resolution of 6’ (nominal WGS84 datum; ~10 km). To remove the orographic effect from PWV maps and to easily visualize the PWV evolution in time, ΔPWV maps were produced in reference to a “calm” moment in which it did not rained, i.e. 02 UTC on 3rd November 2011.
Figure 21 shows the sequence of ΔPWV maps for 4th November 2011, from 00 to 22 UTC. The increase in the amount of water vapor over time in the study area is evident. The Genoa event (black circle in Figure 21) occurred between 9:00 and 13:00 UTC.

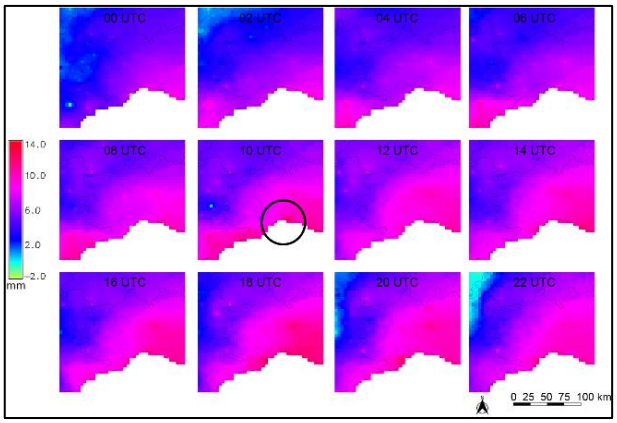

Figure 21. ΔPWV maps for 4th November 2011 (00-22 UTC). The circle indicates the position and time of the higher value.

Higher temporal and spatial resolutions will allow to better localize the event, as discussed in the next section.
However, the PWV value is useful for estimating the maximum amount of rain that can precipitate under triggering conditions. A very rough evaluation of the maximum rain intensity may be obtained by assuming that the raindrops fall with a velocity of 9 m/s (characteristic value for the velocity of large raindrops; see Gunn and Kinzer, 1949) from a typical condensation level altitude of 3000 m; it takes 666 s for the rain drops to reach the ground. Assuming that the PWV remains nearly constant for one hour and that all of the water vapor condenses, the following factor k= 3600/666=5.4, can be considered as multiplying factor relating the PWV values to the maximum amount of potential rain. Thus, the PWV value of 42 mm obtained for 10:00 UTC on November 4, 2011, can be converted into approximately 230 mm/h of potential rain. The DICCA pluviometer at the University of Genoa observed only 75 mm from 9:00 to 10:00 UTC but the Vicomorasso pluviometer in the Bisagno basin betwwen 13 and 14.00 UTC observed 165 mm (see Figure 19b; more details in ARPAL, 2012). Hence, such a rough potential rain computation could be useful for a decision support system based on GNSS meteorology to establish risk thresholds under different rain scenarios.

6.2 PWV near real-time monitoring

The G4M procedure was employed to interpret meteorological events by simulating a near real-time analysis. Indeed, the proposed near real-time analysis is an a posteriori analysis, but it is considered a useful test to evaluate the feasibility of the procedure and its application in near real-time, mainly concerning needed data, computational time, and additional information provided with respect to the a posteriori analysis.
Considering the limited time and space scales of severe meteorological events, typically characterized by short durations (15–30 minutes) and extreme localization (on the order of a few kilometers), a time span of 6 minutes and spatial resolution of 250 m were chosen.
Due to computational limitations in GAMIT software, a 4-hour analysis period and a smaller PSs network were considered. The network consists of the 15 PSs common to the three subnetworks (described in Section 3.1), 14 PSs of the Regione Piemonte network, 6 PSs of the Regione Liguria network, and the EUREF GENO and IGS AJAC PSs as additional stations, as shown in Figure 22.

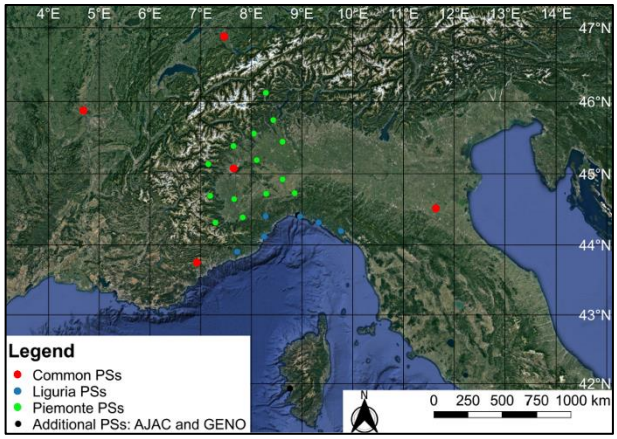

Figure 22. GNSS PSs network for near real-time monitoring

Figure 23 shows a test performed on the accordance of 6 minutes and 2 hours ZTD estimates.

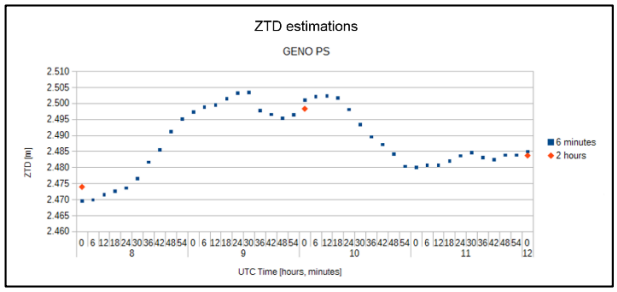

Figure 23. Comparison between 6 minutes and 2 hours ZTD estimates

Slightly different ZTD estimations, in the order of few mm, can be appreciated. Concerning the ZTD rms comparison, higher differences appear, mainly located near the start and the end of session. For this reason, only the three central hours of session have been taken into account, removing the first and the last half hours of the 4 hours session. In general, high rms values could be related to the higher correlation between ZTD estimation in short time span elaborations. Nevertheless, it seems that higher rms values do not influence the interpretation of the time evolution of the investigated meteorological phenomenon. Thus, 6 minutes PWV maps have been obtained starting from 6 minutes ZTD estimations for the severe event occurred on Genoa on 4th November 2011.

Concerning the environmental data, P and T data have been obtained by interpolation of NOAA data, supposing a linear behavior of the temporal evolution of P and T between two sampled data.

A 30-minute extraction of the 6 minutes ΔPWV maps, from 09 to 11:30 UTC on 4th November 2011, is represented in Figure 24.

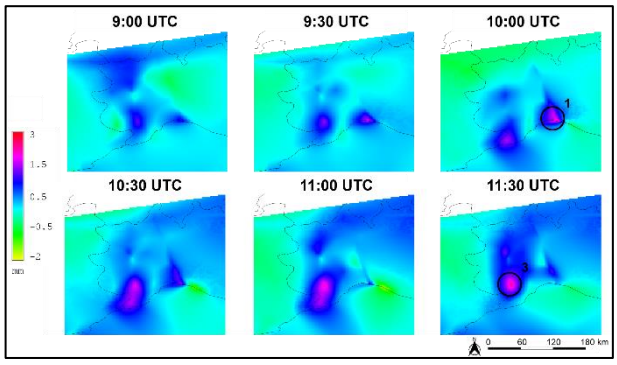

Figure 24. 30-minutes extraction of the 6 minutes ΔPWV maps

The ΔPWV maps were obtained by differentiation in time with respect to 8:30 UTC on November 4, 2011, representing relative "calm" conditions with respect to the rain peak. The ΔPWV maps highlight both positive and negative time differences, corresponding to an increase and decrease in the water vapor amount in the atmosphere, the last one due to rainfall.

In addition to the ΔPWV peak of Genoa, another peak with analogous values is evident in the area around Mondovì (circle 3 in Figure 24), where an intense meteorological event might occur.

HI maps were produced with a spatial resolution of 1 km and a time resolution of 6 minutes from 8:30 to 11:30 UTC on 4th November 2011. A 30-minute extraction from 09 to 11:30 UTC is presented in Figure 25.

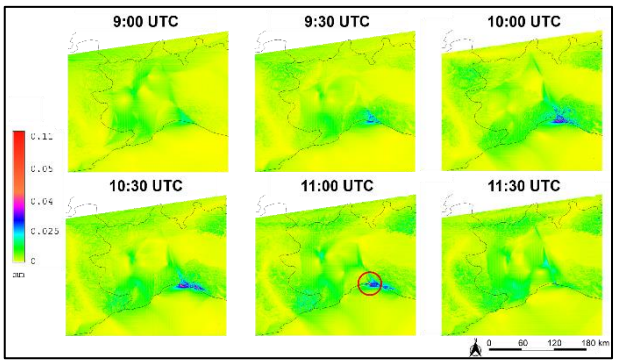

Figure 25. 30-minutes extraction of the 6 minutes HI maps

As expected, the HI maps allow to localize the intense meteorological event, assuming values close to zero for the whole area, except for Genoa, where the event occurred (red circle in Figure 25).

Instead, the ΔPWV peak observed in circle 3 in Figure 24 does not correspond to a high HI value in Figure 25, as expected based on the moderate radar reflectivity in that area (Figure 20).

The timings of the highest HI values (approximately at 11 UTC) in the analyzed time window are in accordance with the highest rain values. HI seems to predict the maximum observed rain, between 11 and 12 UTC, several tens of minutes before. Thus, the locally strong spatial variation in ΔPWV seems to be correlated to the intense meteorological event considered in this study.

The correspondence between HI and the rain peaks will be studied in detail in the near future.

CONCLUSIONS AND FUTURE PERSPECTIVES

The present work focuses on the possibility of obtaining 2D PWV maps starting from GNSS, P and T data coming from existing infrastructure. ZTD is estimated in homogeneous GNSS regional networks, P and T are extracted from international stations in different discrete points. ZTD estimates and P and T observations from international measuring stations are located at different discrete points, with a mean spacing of 40 and 150 km, respectively.

Based on Bevis et al. (1992), a procedure called G4M has been conceived to produce 2D PWV maps with high spatio-temporal resolution (up to 6 min and 250 m for PWV, 1 km for HI).

G4M is based on a simplified mathematical model conceived by the research group, which is able to effectively describe the 2D P and T fields, despite difficulties due to the sparse distribution of observed data.

The procedure was applied to an area approximately covering northwestern Italy, to study a severe meteorological event that occurred in Genoa on 4th November 2011.

The strength and originality of the G4M procedure are based on the use of existing infrastructure, the independence from meteorological models, the possibility of automation, the high adaptability to different network configurations, and the ability to produce high-resolution 2D PWV maps, even from sparse input data.
A comparison has been carried out both in 1D and 2D on the different interpolation techniques for ZTD, P and T in order to state the most appropriate interpolation technique in sight of applying the G4M procedure in near real-time. Moreover, P, T and PWV fields obtained via G4M have been validated by comparison with those originating from WRF meteorological simulations.
The study of PWV time series for PSs at different altitudes, the evaluation of PWV behavior along a section crossing complex topography, and the computation of difference maps between G4M and WRF PWV fields led to understand that the encouterd differences do not influence the interpretation of the meteorological phenomenon evolution in time. Hence, the procedure can be considered effective. The emerged key role of orography can be roughly removed by introducing the ΔPWV map, representing the differentiation of the PWV in time with respect to a "calm" moment. The observation of different PWV values over time provides the spatial and temporal evolution of the PWV, allowing for easier monitoring of the atmosphere.
The HI, conceived by the research group, allows to localize of severe meteorological events in time and space, accounting for the spatial variability of ΔPWV. It allows to discriminate between locations and times characterized by high ΔPWV values based on spatial ΔPWV heterogeneity, which seems to be correlated with the intense meteorological event considered in this study.
The G4M procedure has been applied both to a posteriori and simulated near real-time strategies using 2-hour and 6-minute ZTD, P, and T data. The simulated near real-time strategy and the analysis of HI evolution during the analysed event seem to be promising for a future early-warning system based on G4M. In fact, because the entire G4M procedure is independent from meteorological models, it could be innovatively integrated into them, supporting now-casting.
Systematic application of G4M procedure to different case studies (intense and moderate events, lacking/false meteorological alerts) to statistically evaluate the reliability of HI and its performance is planned for the near future. Moreover, the relationship between HI and rain peaks will be studied in depth.

ACKNOWLEDGEMENTS

I wish to thank:
- prof. Bianca Federici and prof. Domenico Sguerso for supervising this thesis;
- prof. Toshitaka Tsuda and prof. Giovanna Venuti for being the external reviewers of this PhD thesis;
- prof. Andrea Walpersdorf for hosting me at ISTerre to work with her on RENAG Database update;
- prof. Andrea Mazzino and Dr. Federico Cassola for sharing the meteorological simulation data.

REFERENCES

ARPAL (2012) Genoa November 4-9, 2011 meteo-hydrological event report. Quaderni ARPAL, n.2 (in Italian; https://www.arpal.gov.it/images/stories/meteo/Documenti_sito/QuadernoArpalGenovaSettembre_WEB.pdf)

Basili P., Bonafoni S., Ferrara R., Ciotti P., Fionda E., Betti B., Prini R., Tornatore V., Crespi M., Di Paola S., Baiocchi V., Radicioni F. (2003). Assessment of precipitable water vapour by use of a local GPS network and microwave ground-based radiometer. 11th International Conference on Antennas and Propagation (ICAP 2001), vol. 2001, p. 72-76, Institute of Electrical and Electronics Engineers Inc., ISBN: 0852967330, doi: 10.1049/cp:20010241

Bennitt G.V., Jupp A. (2012). Operational Assimilation of GPS Zenith Total Delay Observations into the Met Ofce Numerical Weather Prediction Models. Monthly Weather Review, 140, pp. 2706–2719

Bevis M., Businger S., Herring T., Rocken C., Anthes R., Ware R. (1992). GPS meteorology – Remote sensing of atmospheric water vapor using the Global Positioning System. Journal of Geophysical Research, 97, pp. 15787–15801

Bevis M., Businger S., Chiswell S., Herring T., Anthes R., Rocken C., Ware R. (1994). GPS meteorology: Mapping zenith wet delays onto precipitable water. Journal of applied meteorology, 33, pp. 379–386

Bock O., Bouin M.N., Doerfinger E., Collard P., Masson F., Meynadier R., Nahmani S., Koité M., Balawan K.G.L., Didé, F., Ouedraogo D., Pokperlaar S., Ngamini J.B., Lafore J.P., Janicot S., Guichard F., Nuret M. (2008). West African Monsoon observed with ground-based GPS receivers during African Monsoon Multidisciplinary Analysis (AMMA). Journal of Geophysical Research, 113, doi: 10.1029/2008JD010327

Boniface K., Ducrocq V., Jaubert G., Yan X., Brousseau P., Masson F., Champollion C., Chéry J., Doerfinger E. (2009). Impact of high-resolution data assimilation of GPS zenith delay on Mediterranean heavy rainfall forecasting. Annales Geophysicae, 27(7), pp. 2739–2753, doi: 10.5194/angeo-27-2739-2009

Bosy J., Kaplon J., Rohm W., Sierny J., Hadas T. (2012). Near real-time estimation of water vapour in the troposphere using ground GNSS and the meteorological data. Annales Geophysicae; Katlenburg-Lindau30.9: 1379

Bouma H.R., Stoew B. (2001). GPS observations of daily variations in the atmospheric water vapor content. Physics and Chemistry of the Earth, Part A: Solid Earth and Geodesy, 26, pp. 389–392

Cassola F., Ferrari F., Mazzino A. (2015). Numerical simulations of Mediterranean heavy precipitation events with the WRF model: a verification exercise using different approaches. Atmospheric Research, 164-165, pp. 210-225

Crespi M., Luzietti L., Frattale Mascioli F., Rizzi A. (2004). Impiego meteorologico del GPS per la previsione di precipitazioni critiche. In: 8° Conferenza Nazionale ASITA. Federazione Italiana delle Associazioni Scientifche per le Informazioni Territoriali ed Ambientali, Roma, 14-17 dicembre, 2004

Davis J.L., Herring T.A., Shapiro I.I., Rogers A.E.E., Elgered G. (1985). Geodesy by interferometry: effects of atmospheric modeling errors on estimates of baseline lengths. Radio Science 20, pp. 1593-1607

De Pondeca M.S.F.V., Zou X. (2001). A Case Study of the Variational Assimilation of GPS Zenith Delay Observations into a Mesoscale Model. Journal of Applied Meteorology, 40, pp. 1559–1576

Elgered G., Davis J.L., Herring T.A., Shapiro I.I. (1991), Geodesy by radio interferometry: Water vapor radiometry for estimation of the wet delay, J. Geophys. Res., 96, pp. 6541-6555

Ferrando I., Federici B., Sguerso D. (2017). Zenith total delay interpolation to support GNSS monitoring of potential precipitations. GEAM - Geoingegneria Ambientale e Mineraria, Anno LIV, n. 2, pp. 85-90

Ferrando I., De Rosa P., Federici B., Sguerso D. (2016). Spatial interpolation techniques for a near real-time mapping of Pressure and Temperature data. PeerJ Preprints 4:e2223v2 https://doi.org/10.7287/peerj.preprints.2223v2

GRASS Development Team. (2010). Geographic Resources Analysis Support System (GRASS) Software, Version 6.4.0. Open Source Geospatial Foundation http://grass.osgeo.org

Gunn R., Kinzer G.D. (1949). The terminal velocity of fall for water droplets in stagnant air. Journal of Meteorology, 6(4), pp. 243-248

Herring T.A., King R.W., McClusky S.C. (2010). GAMIT Reference Manual–Release 10.4. Department of Earth, Atmospheric, and Planetary Sciences, Massachusetts Institute of Technology. ed. USA

Herring T.A., King R.W., McClusky S.C. (2015). GAMIT Reference Manual–Release 10.6. Department of Earth, Atmospheric, and Planetary Sciences, Massachusetts Institute of Technology. ed. USA

Karabatić A., Weber R., Hayden T. (2011). Near real-time estimation of tropospheric water vapour content from ground based GNSS data and its potential contribution to weather now-casting in Austria. Advances in Space Research, Volume 47, Issue 10, Pages 1691-1703

Pacione R., Vespe F. (2003). GPS Zenith Total Delay Estimation in the Mediterranean Area for Climatological and Meteorological Applications. Journal of Atmospheric and Oceanic Technology, Vol. 20, 1034.

Piccardo D., Sguerso D. (2007). Il contributo del GPS nelle previsioni di eventi meteorologici significativi. Atti della 11° Conferenza Nazionale ASITA, Torino, 6-9 novembre 2007, vol. 2, pp. 1775-1780

R Development Core Team. (2008). R: A language and environment for statistical computing. R Foundation for Statistical Computing, Vienna, Austria. ISBN 3-900051-07-0, http://www.R-project.org

Resch G.M. (1984). Water vapor radiometry in geodetic applications, Geodetic Refraction, pp. 53-84

RENAG DataBase ftp://renag.unice.fr//products/GPS_climatology_Sguerso_Labbouz_Walpersdorf

Saastamoinen J. (1972). Introduction to practical computation of astronomical refraction. Bulletin Géodésique, 106, pp. 383-397

Santerre R. (1991). Impact of GPS satellite sky distribution. Manuscripta Geodaetica, 16, pp. 28-53

Sato K., Realini E., Tsuda T., Oigawa M., Iwaki Y., Shoji Y., Seko H. (2013). A high-resolution Precipitable Water Vapor monitoring system using a dense network of GNSS receivers. Journal of Disaster Research, 8(1), pp. 37-47

Sguerso D., Labbouz L., Walpersdorf A. (2013). 14 years of GPS tropospheric delays in the French-Italian border region: a data base for meteorological and climatological analyses. The International Archives of the Photogrammetry, Remote Sensing and Spatial Information Sciences, XL-5/W3, 7-14, doi:10.5194/isprsarchives-XL-5-W3-7-2013

Sguerso D., Federici B., Agrillo G., Ferrando I. (2014). Il contributo della geomatica alla valutazione delle allerte meteorologiche. Newton's Bulletin, ISSN 1810-8563, Volume: Il prof. Sansò e l'evoluzione della geodesia in Italia, CD-ROM, pp. 1-11

Sguerso D., Labbouz L., Walpersdorf A. (2015). 14 years of GPS tropospheric delays in the French–Italian border region: comparisons and first application in a case study, Applied Geomatics, DOI 10.1007/s12518-015-0158-z, ed. Springer Verlag, Online ISSN 1866-928X, pp. 1-13

Sieczka M. and GRASS Development Team 2006. r.surf.nnbathy GRASS Software, Version 6.4. Open Source Geospatial Foundation

Solheim F.S., Vivekanandan J., Ware R.H., Rocken C. (1999). Propagation delays induced in GPS signals by dry air, water vapor, hydrometeors, and other particulates. Journal of Geophysical Research, 104, pp. 9663-9670

Spilker J.J. (1980). Signal structure and performance characteristics, Navigation, 1, Institute of Navigation, pp. 29-54

Tralli D.M., Dixon T.H., Stephens S. (1988). The effect of wet tropospheric path delays on estimation of geodetic baselines in the Gulf of California using the Global Positioning System, J. Geophys. Res., 93, pp. 6545-6557

Tregoning P., Boers R., O'Brien D. (1998). Accuracy of absolute precipitable water vapor estimates from GPS observations. Journal of Geophysical Research: Atmospheres, 103(D22), pp. 28701-28710

Tsuda T., Sato K., Realini E., Oigawa M., Iwaki Y., Shoji Y., Seko H. (2013). A real-time monitoring system of Precipitable Water Vapor (PWV) using a dense GNSS receiver network. Journal of Disaster Research, vol.8 No.1, pp. 155-156

Walpersdorf A., Bouin M.N., Bock O., Doerflinger E. (2007). Assessment of GPS data for meteorological applications over Africa: Study of error sources and analysis of positioning accuracy. Journal of Atmospheric and Solar-Terrestrial Physic, 69(12), pp. 1312-1330

Yao Y., Xu C., Shi J., Cao N., Zhang B., Yang J. (2015). ITG: A New Global GNSS Tropospheric Correction Model. Sci. Rep. 5, 10273; doi: 10.1038/srep10273.